Journal of
Biomaterials and Tissue Engineering
Vol. 12, 1683–1691, 2022

Preparation of g-C_3N_4/CQDs/Ag_2S Composite Material and Its Antibacterial Properties

Hongxia Li[1], Xiang Gao[1], Xiaohui Niu[1], Deyi Zhang[1], Haiyan Fan[2,*], and Kunjie Wang[1,*]

[1] *College of Petrochemical Technology, Lanzhou University of Technology, Lanzhou, 730050, China*
[2] *Chemistry Department, Nazarbayev University, Astana, 010000, Kazakhstan*

The emergence of bacterial resistance to traditional antibiotics and its global spread has brought huge threats to human life and health, and the need for new alternative antibacterial agents has become increasingly urgent. The rapid development of nanoscience provides a potential alternative to antibacterial therapy. In this study, g-C_3N_4 was synthesized using melamine as the raw material. It was then successfully combined with carbon quantum dots (CQDs) and silver sulfide to synthesize a g-C_3N_4/CQDs/Ag_2S composite material. Such combination narrows the band gap of g-C_3N_4 from 2.53 eV to 2.21 eV and enhances the photocatalytic efficiency. Consequently, it indicated photocatalytic antimicrobial effects against three strands of bacteria, *Shylococcus aureus* (Gram-positive), *Escherichia coli* (Gram-negative) and Methicillin-resistant *Staphylococcus aureus* under the irradiation of visible light. Other than the common pathogens, g-C_3N_4/CQDs/Ag_2S exhibited an appreciable inhibition against the well-known drug-resistant bacteria. With its antimicrobial features and excellent photoelectric properties, the as prepared nanocomposites show its potential in the development of new antimicrobial and photocatalytic materials.

Keywords: g-C_3N_4, Carbon Quantum Dots, Ag_2S, Antibacterial Agent.

RESEARCH ARTICLE

1. INTRODUCTION

The antibacterial therapy provided by nanocomposites with photocatalytic properties has been widely practiced.[1–3] Such antimicrobial effect is achieved through the absorption of energy from light irradiation leading to the production of reactive oxygen species (ROS) through photoinduced electrons.[4,5] The generated ROS are able to simultaneously attack various cellular sites such as nucleic acids, proteins and lipids in pathogens,[6,7] and therefore induce a non-specific inhibition against the bacterial growth, which potentially reduces the chances for the development of drug resistance.[8,9] Among nanomaterials indicating antimicrobial effects, the ones with heterostructure exhibit unique optical properties reflected in the increased light absorption and the expansion of the absorption area,[10,11] resulting in excellent antibacterial activities.[12]

As a metal-free conjugated semiconductor,[13,14] graphite phase carbon nitride (g-C_3N_4) has attracted much attention for its applications as an antibacterial agent.[15] Containing only two elements, carbon and nitrogen, g-C_3N_4 can be produced using low-cost methods.[16] Being a metal-free semiconductor,[17] g-C_3N_4 indicates a good biocompatibility. Along with a narrow band gap,[18,19] g-C_3N_4 becomes an ideal candidate of the photodynamic antibacterial. However, due to the short lifetime of the photogenerated electron-holes before recombination, advantages of g-C_3N_4 have not been fully taken.[20–23] A potential solution is to dope with compound semiconductors to form a heterostructure with g-C_3N_4, which generally narrowed the band gap and further improved photocatalytic performance.[24–26]

Silver sulfide, a very common semiconductor, possesses a large absorption coefficient,[27] and a band gap of ~1.0 eV.[28] With its good photocatalytic performance under visible light and near-infrared light,[29,30] silver sulfide has been widely used in the fields of hydrogen release, organic pollution degradation, and bioimaging.[31] On the other hand, carbon quantum dots (CQDs) have shown excellent electrical conductivity and suppressing the recombination of photoinduced charge carriers, therefore have been introduced to the photocatalytic composite.[32–34]

The strategy of the present work is to combine the virtues of g-C_3N_4, Ag_2S and CQDs to form a heterostructure, which potentially possesses narrow band gap and long lived photoinduced electrons and holes. Thus the produced composite with such heterostructure may indicate higher photocatalytic efficiency to promote the production of active oxygen, and thereby enhance the photocatalytic antibacterial activity.

*Authors to whom correspondence should be addressed.

We synthesized g-C_3N_4 through simple heating treatment doped with silver sulfide and carbon quantum dots using an in-situ growing method. The morphology, chemical compositions and photocatalytic properties of the as prepared g-C_3N_4/CQDs/Ag_2S composite material were characterized, and the antimicrobial effect was tested on three stripes of bacteria including *Staphylococcus aureus*, *Escherichia coli* and *Staphylococcus aureus*.

2. EXPERIMENTAL DETAILS

2.1. Materials

Sodium hydroxide (NaOH), acetone (CH_3COCH_3), hydrochloric acid (HCl), sodium sulfide (Na_2S), sodium citrate ($Na_3C_6H_5O_7 \cdot 2H_2O$), silver nitrate ($AgNO_3$) were purchased from Sinopharm Group Co. Ltd. (Shanghai, China); melamine was purchased from Aladdin Chemistry, Shanghai; the gram-negative bacteria (*Escherichia coli*), gram-positive bacteria (*Staphylococcus aureus*) and drug-resistant bacteria (methicillin-resistant *Staphylococcus aureus*) were obtained from the Microbiology Department of Lanzhou Maternal and Child Health Care Hospital.

2.2. Preparation of g-C_3N_4/CQDs/Ag_2S Composite Materials

Ag_2S and CQDs were synthesized using the methods described in our previous work.[35] The preparation of g-C_3N_4 was based on the reported method using melamine as the starting material.[36] The composite of g-C_3N_4/CQDs/Ag_2S was prepared by *in-situ* growth of Ag_2S and CQDs on the surface of g-C_3N_4 at room temperature. Added 0.1 g of the processed g-C_3N_4, 10 mL of 0.1 mol/L silver nitrate solution to 10 mL of 0.05 mol/L sodium citrate solution. The mixture was sonicated for 5 minutes followed by the addition of 20 mL of 0.05 mol/L sodium sulfide solution under stirring, continued to stir for 4 h. Upon addition of 0.05 g of CQDs to the mixed solution and stirred for 4 h, the product was collected, washed with distilled water and absolute ethanol and dried in an oven at 60 °C for 12 h (Scheme 1).

2.3. Characterization

The XRD spectra in the range of 5.0° to 80.0° were recorded at a scanning rate of 5.0°/min Using Shimadzu 17-XRD6000 X-ray diffractometer (XRD). Surface functional groups were characterized through FT-IR spectroscopy using a Nicolet AVTAR 360FT-IR spectrometer. These functional groups were further confirmed by X-ray photoelectron spectroscopy (XPS). The morphologies of the each component and the composites were identified using JEOL JEM2100 high resolution transmission electron microscope (HR-TEM).

2.4. Ultraviolet Visible Diffuse Reflectance Spectrum Test

Due to the difference in the composition and structure of the material, the absorption degree of ultraviolet and visible light is different, which has an important influence on its photocatalytic activity. Therefore, we analyze and determine the light absorption performance of the prepared material. The UV-vis diffuse reflectance spectrum was recorded by V-1800 visible spectrophotometer.

2.5. Photoelectrochemical Analysis

CHI600E conventional three-electrode electrochemical workstation was used to detect the photocurrent response and electrochemical impedance of the prepared g-C_3N_4/CQDs/Ag_2S composite material. Using 0.1 M Na_2SO_4 aqueous solution as the electrolyte, the photoelectric catalytic performance of the product was tested.

2.6. Antibacterial Activity Test

The *in vitro* antibacterial tests were referred to the methodologies described in our previous work.[37]

3. RESULTS AND DISCUSSION

3.1. Structure and Chemical Composition

The FT-IR spectra of different materials are presented in Figure 1(a). For g-C_3N_4, the band at 1637 cm^{-1} is assigned as the C═N stretching vibration, whereas peaks centered at 1252, 1323, 1407 cm^{-1} and 1465 cm^{-1} are identified as the aromatic CN stretching vibration; the characteristic peak at 808 cm^{-1} is attributed to the stretching of the triazine unit.[38] The broad peak centered at 3188 cm^{-1} represents the stretching vibration of the N–H bond. The FT-IR spectrum of CQDs indicates a broad absorption centered at 3419 cm^{-1} due to the stretching vibration of the associated –OH; the absorption peak near 1575 cm^{-1} corresponds to the C═O stretching on the deprotonated carboxylic group. In the FT-IR spectrum of g-C_3N_4/CQDs, the characteristic absorption bands representing C═N stretching, C═O stretching, aromatic CN stretching are observed and showing no significant shift in frequency compared to g-C_3N_4 and CQDs indicating a

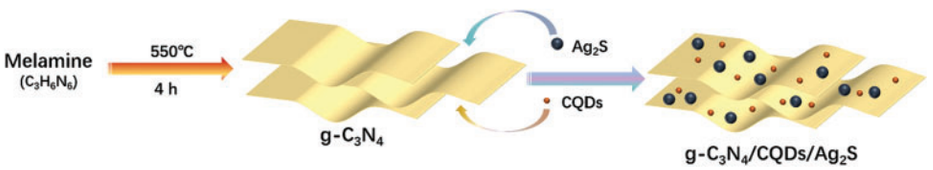

Scheme 1. The mechanism for the formation of g-C_3N_4/CQDs/Ag_2S.

RESEARCH ARTICLE

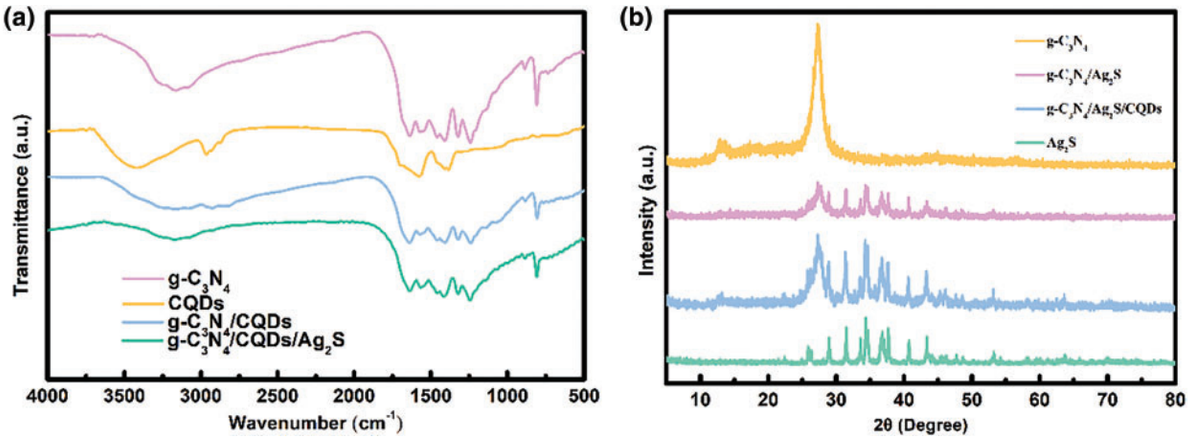

Fig. 1. (a) FTIR spectra of different materials; (b) XRD spectra of different materials.

successful loading of CQDs on g-C_3N_4. Meanwhile, no significant difference was observed in the FT-IR spectrum of g-C_3N_4/CQDs/Ag_2S from that of g-C_3N_4/CQDs indicating that Ag_2S and CQDs did not cause structural changes of g-C_3N_4 during the compounding process.

The XRD patterns of g-C_3N_4 (Fig. 1(b)) exhibit two diffraction peaks at 2θ of 13.04° and 27.47° correspond to the (100) and (002) peaks of the graphite phase material respectively, an indication of the in-plane stacking structure and the interlayer accumulation of aromatic chain segments. Upon doping of Ag_2S, these two peaks are attenuated, and the characteristic peaks of silver sulfide appears in a good agreement with the standard card PDF#14-0072 of Ag_2S, indicating that Ag_2S nanoparticles have been successfully loaded on the surface of g-C_3N_4. The XRD diffraction pattern of g-C_3N_4/CQDs/Ag_2S after loading CQDs shows small peaks near 15° corresponding to the graphitization peak in CQDs, indicating that CQDs and Ag_2S were successfully composited on g-C_3N_4.

The survey XPS spectrum of g-C_3N_4 (Fig. 2(a)) shows three main peaks corresponding to C, N and O elements. Two peaks at 284.8 eV and 287.4 eV are deconvolved from the high resolution spectrum of C 1*s* (Fig. 2(b)) correspond to C–N–C group and N–C=N group in g-C_3N_4,[39,40] whereas three featured peaks at 398 eV, 398.9 eV and 400 eV are observed for the high resolution scan of N 1*s* (Fig. 2(c)), which are recognized as C–N–C, N–(C)3 and C–NH_2 groups respectively.[41,42]

Other than the peaks representing C, N and O elements, peaks of Ag and S appeare on the XPS survey spectrum of g-C_3N_4/CQDs/Ag_2S (Fig. 3(a)). The high-resolution X-ray photoelectron spectrum of C 1*s* (Fig. 3(b)) exhibits two peaks at 284.7 eV and 288.3 e. The new peak centered at 288.3 eV compared to that of g-C_3N_4 is mainly due to N–C=N in CQDs indicating that CQDs are distributed on the surface of g-C_3N_4.[43] Two peaks at 531.5 eV and 532.6 eV in O 1*s* high resolution spectrum (Fig. 3(c)) are identified as C–O–C and C–OH due to CQDs.[44] The high-resolution scan of N 1*s* for g-C_3N_4/CQDs/Ag_2S (Fig. 3(d)) missed the peak at 398 eV compared to that of g-C_3N_4 indicating CQDs may occupy the position where C–N–C groups are located. The high-resolution peaks for Ag 3*d* (Fig. 3(e)) at 367.9 eV and 373.9 eV are attributed to the binding energies of Ag $3d_{5/2}$ and Ag $3d_{3/2}$, respectively. The secondary peaks corresponding to S $2p_{3/2}$ and S $2p_{1/2}$[45] at approximately 162.1 eV and 160.8 eV (Fig. 3(f)), are identified as the sulfur anions in the Ag_2S lattice. The results from XRD, FT-IR and XPS confirm the chemical compositions of the as prepared composite.

The EDS spectra of g-C_3N_4/CQDs/Ag_2S (Fig. 4) visualize the distribution of the C, O, N, Ag, and S elements on the surface of the composite. The even distribution of each element across the surface of the detected composite indicates the intrinsic binding among g-C_3N_4, CQDs and Ag_2S in g-C_3N_4/CQDs/Ag_2S composite.

The morphology of the g-C_3N_4/CQDs/Ag_2S composite is revealed in the TEM images (Figs. 5(a and b)). A flaky structure with a dimension of micrometer is identified with the CQDs distributed on the surface. The HRTEM image (Fig. 5(c)) shows CQDs with a size of about 3 nm are deposited on the surface of the g-C_3N_4 sheet with a lattice fringe spacing is 0.268 nm, corresponding to the (120) crystal plane of silver sulfide implying the Ag_2S nanoparticles are well incorporated in the composite system.

3.2. Photodynamic Performance of g-C_3N_4/CQDs/Ag_2S Composite

The light absorption properties of pure g-C_3N_4, Ag_2S and g-C_3N_4/CQDs/Ag_2S composite materials were analyzed by ultraviolet-visible diffuse reflectance spectroscopy. The absorption edge of the g-C_3N_4 sample is observed at 460 nm (Fig. 6(a)). The UV-Vis spectrum of pure Ag_2S is basically the same as that of Ag_2S reported in the literature.[46] The absorption edge of g-C_3N_4/CQDs/Ag_2S composite material is located between 460 and 490 nm. The loading of CQDs and Ag_2S leads to the absorption edge of the g-C_3N_4/CQDs/Ag_2S moving to a longer

RESEARCH ARTICLE

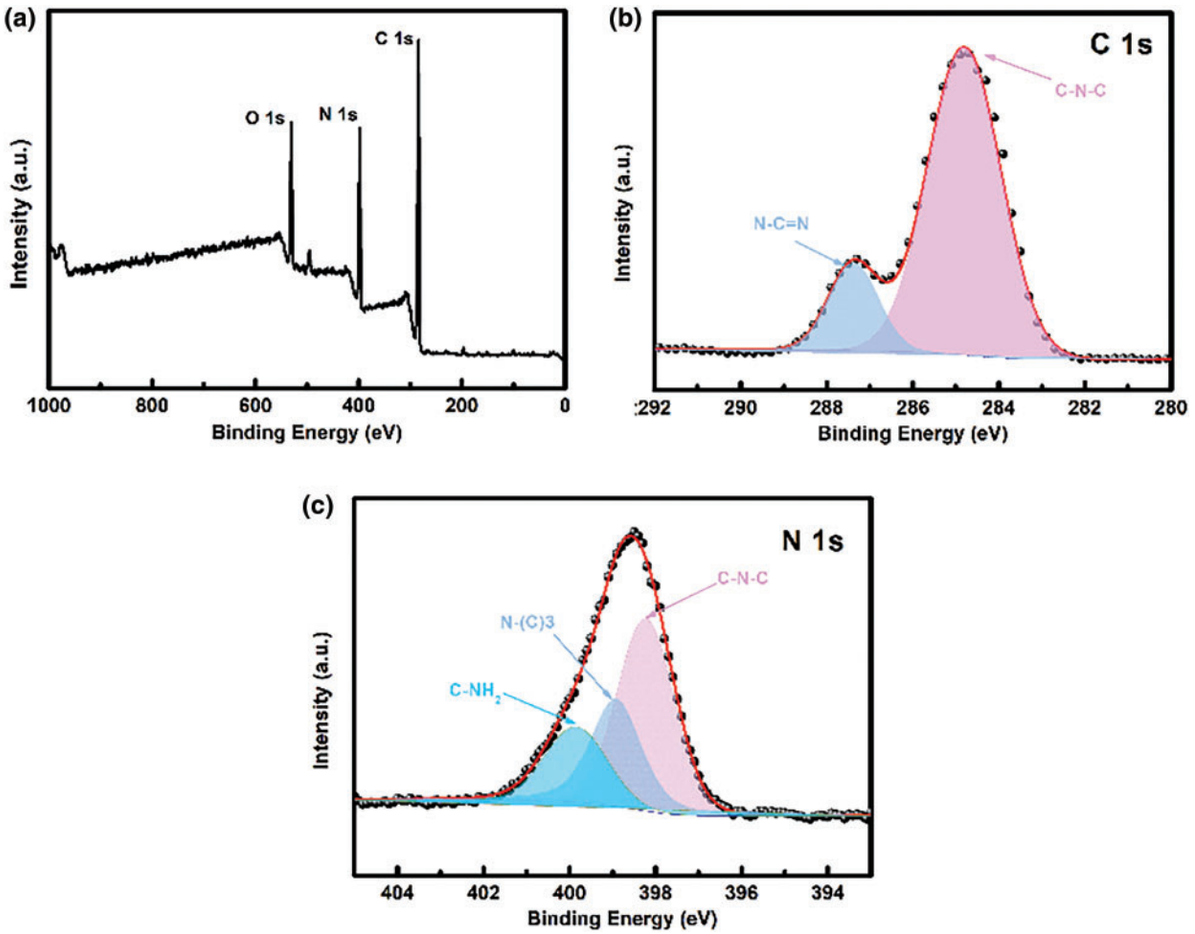

Fig. 2. (a) XPS spectrum of g-C_3N_4, (b) C 1*s*, (c) N 1*s*.

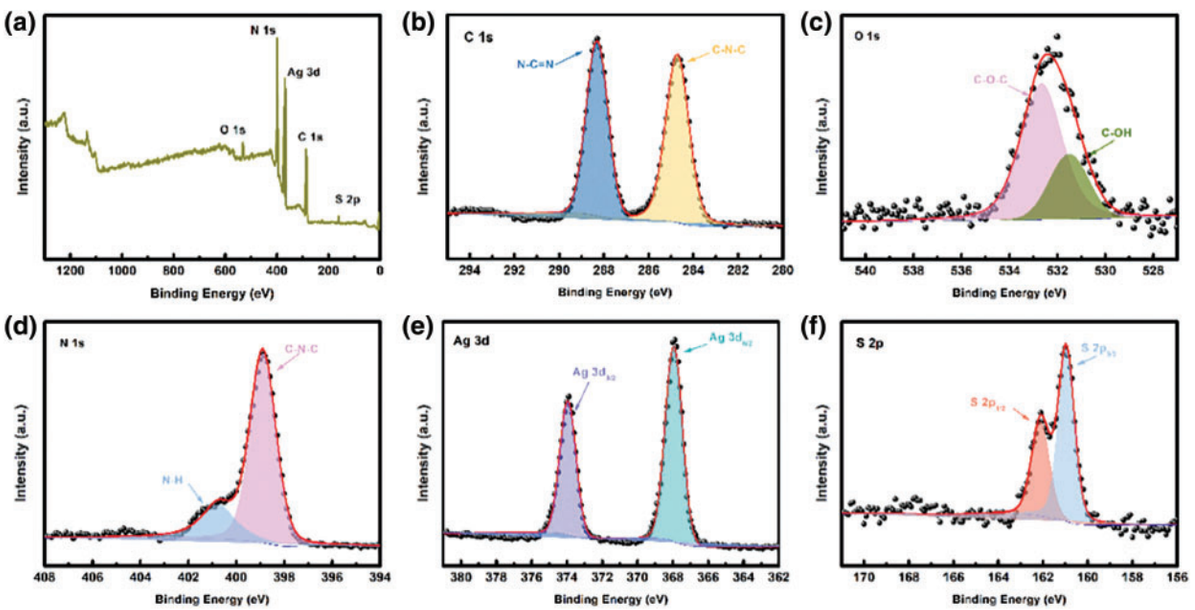

Fig. 3. (a) XPS spectrum of g-C_3N_4/CQDs/Ag_2S, (b) C 1*s*, (c) O 1*s*, (d) N 1*s*, (e) Ag 3*d*, (f) S 2*p*.

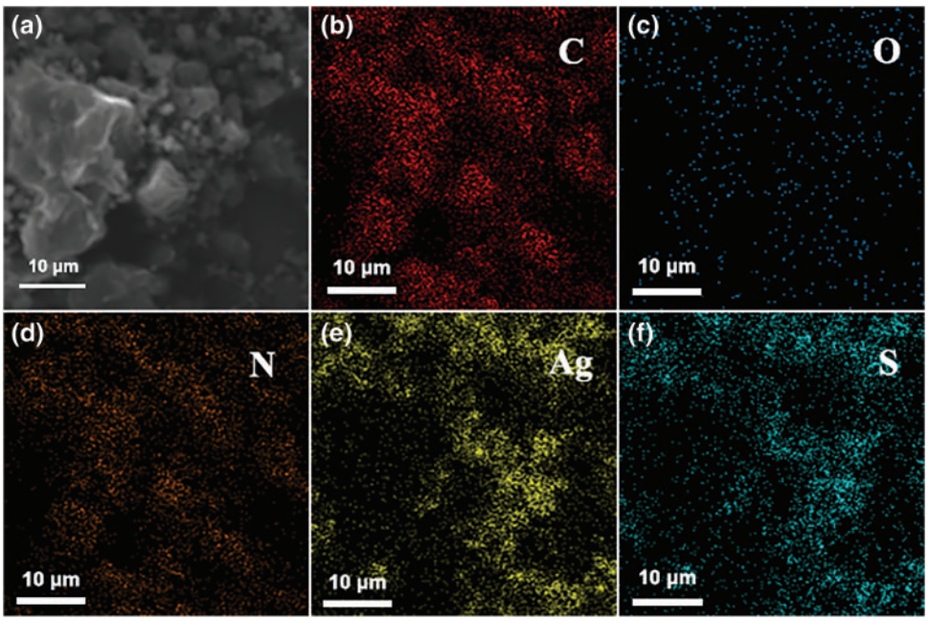

Fig. 4. EDS element distribution of g-C_3N_4/CQDs/Ag_2S, (b) C element, (c) O element, (d) N element, (e) Ag element, (f) S element.

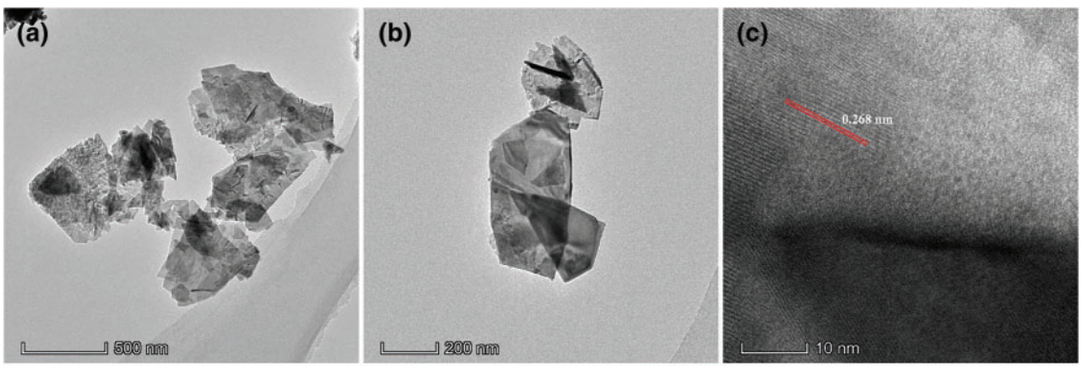

Fig. 5. TEM image of g-C_3N_4/CQDs/Ag_2S.

wavelength. The band gap energy was derived using the equation below,

$$\alpha h\nu = A\left(h\nu - E_g\right)^{n/2}$$

wherein, α, h, ν, A and E_g represent absorption coefficients, optical frequency and band gap respectively. Among them, n is determined according to the type of optical transition of the semiconductor ($n = 1$ means direct transition, $n = 4$ means indirect transition). Referring to the relevant literature,[47] the n values for g-C_3N_4 and Ag_2S are 4 and 1, respectively. Combining the experimental data, the band gap for g-C_3N_4 is calculated as 2.5 eV, for g-C_3N_4/CQDs/Ag_2S, 2.2 eV (Fig. 6(b)).

To characterize the stability of the photoinduced carriers of g-C_3N_4/CQDs/Ag_2S composite, the photoelectrochemical measurements including photocurrent response and electrochemical impedance were performed. The photocurrent response tests indicate the photocurrent density of the original g-C_3N_4 is the smallest, and that of g-C_3N_4/Ag_2S is slightly higher. The g-C_3N_4/CQDs/Ag_2S composite exhibits a significant increase in photocurrent density showing the critical role of CQDs, as the photocurrent density is a measure of population of photogenerated electrons and holes. It is evident, that small particles of CQDs distributed on the g-C_3N_4 sheet provide a larger surface for the distribution of photogenerated charge carriers. Moreover, the particles of CQDs can stabilize the photogenerated electrons, holes or both through its surface functional groups, which often carry positive/negative change.

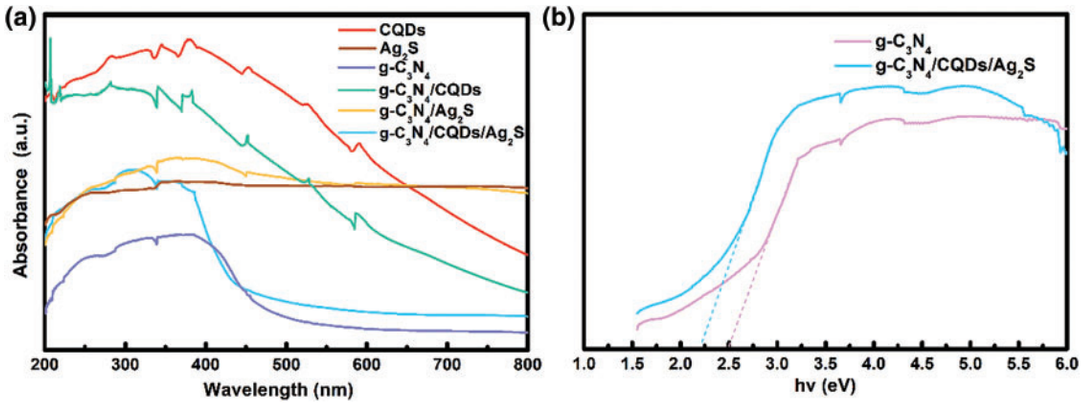

Fig. 6. (a) UV-Vis diffuse reflectance spectra of different materials; (b) The band gap of g-C_3N_4 and g-C_3N_4/CQDs/Ag_2S.

The charge transfer resistance was measured using EIS, a significant decrease in radius is observed (Fig. 7(b)) for g-C_3N_4/CQDs/Ag_2S, indicating that the g-C_3N_4/CQDs/Ag_2S composite has low impedance and fast interface charge transfer due to the large surface area provided by CQDs distributed on the flaky surface of g-C_3N_4 and Ag_2S.

3.3. Analysis of Antibacterial Properties of g-C_3N_4/CQDs/Ag_2S Composite

The antibacterial properties of different materials under the light and the dark conditions are displayed in Figure 8. Upon irradiation, no obvious antimicrobial effect is observed for both Ag_2S and g-C_3N_4; CQDs/g-C_3N_4 shows weak antibacterial effect; treatment with CQDs/Ag_2S and Ag_2S/g-C_3N_4, indicates the decrease in the number of colonies; treatment with g-C_3N_4/CQDs/Ag_2S composites demonstrates the most significant antibacterial effect.

The contrast between the results in light and dark reveals the antimicrobial effect in the present work is related to the photoelectric activities of the as prepared composites. Due to its large forbidden band width and short-lived photoinduced electrons and holes, g-C_3N_4 indicates little photoelectric activity. Ag_2S, on the other hand, although with narrower bandgap, possesses low photoelectric efficiency because of the immediate recombination of the photo-generated electron–holes before generating significant amount of active oxygen. Thus, g-C_3N_4 or Ag_2S alone shows rather poor antimicrobial effects. Participating of Ag_2S in Ag_2S/g-C_3N_4 and Ag_2S/CQDs complexes leads to the formation of binary heterojunctions, further, band hybridization, which helps to enhance the photoelectric efficiency and consequently, the production of more active oxygen under irradiation of the visible light to achieve decent antibacterial effect. The heterostructure formed in g-C_3N_4/CQDs/Ag_2S holds the virtues of narrower band gap than that of g-C_3N_4 and the prolonged lifetime of photoinduced electron–hole due to the stabilization provided by CQDs, therefore produce more active oxygen which greatly improve the antibacterial performance.

3.4. Analysis of Antibacterial Mechanism of g-C_3N_4/CQDs/Ag_2S Composite

Based on the analysis above, the antimicrobial properties of the g-C_3N_4/CQDs/Ag_2S composite can be featured with a photocatalytic mechanism. The diagram in Figure 9

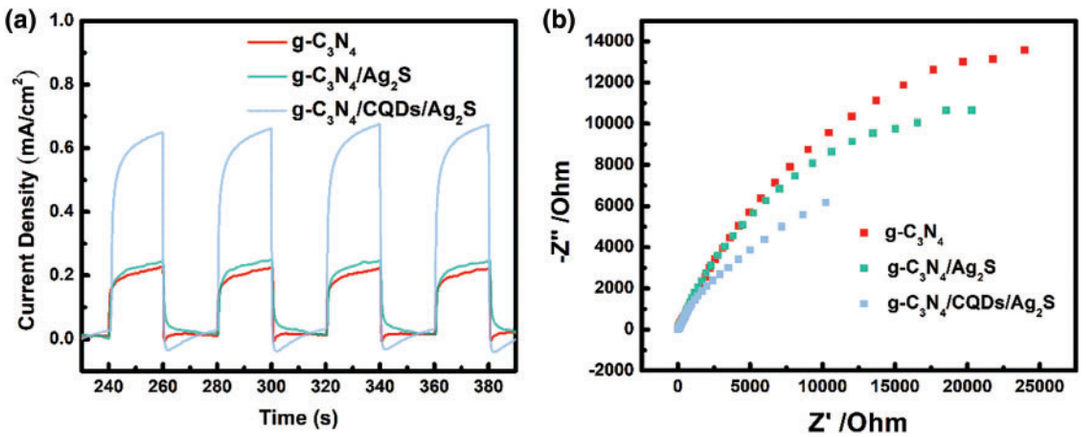

Fig. 7. (a) Photocurrent response and (b) Electrochemical impedance of g-C_3N_4, g-C_3N_4/Ag_2S and g-C_3N_4/CQDs/Ag_2S.

RESEARCH ARTICLE

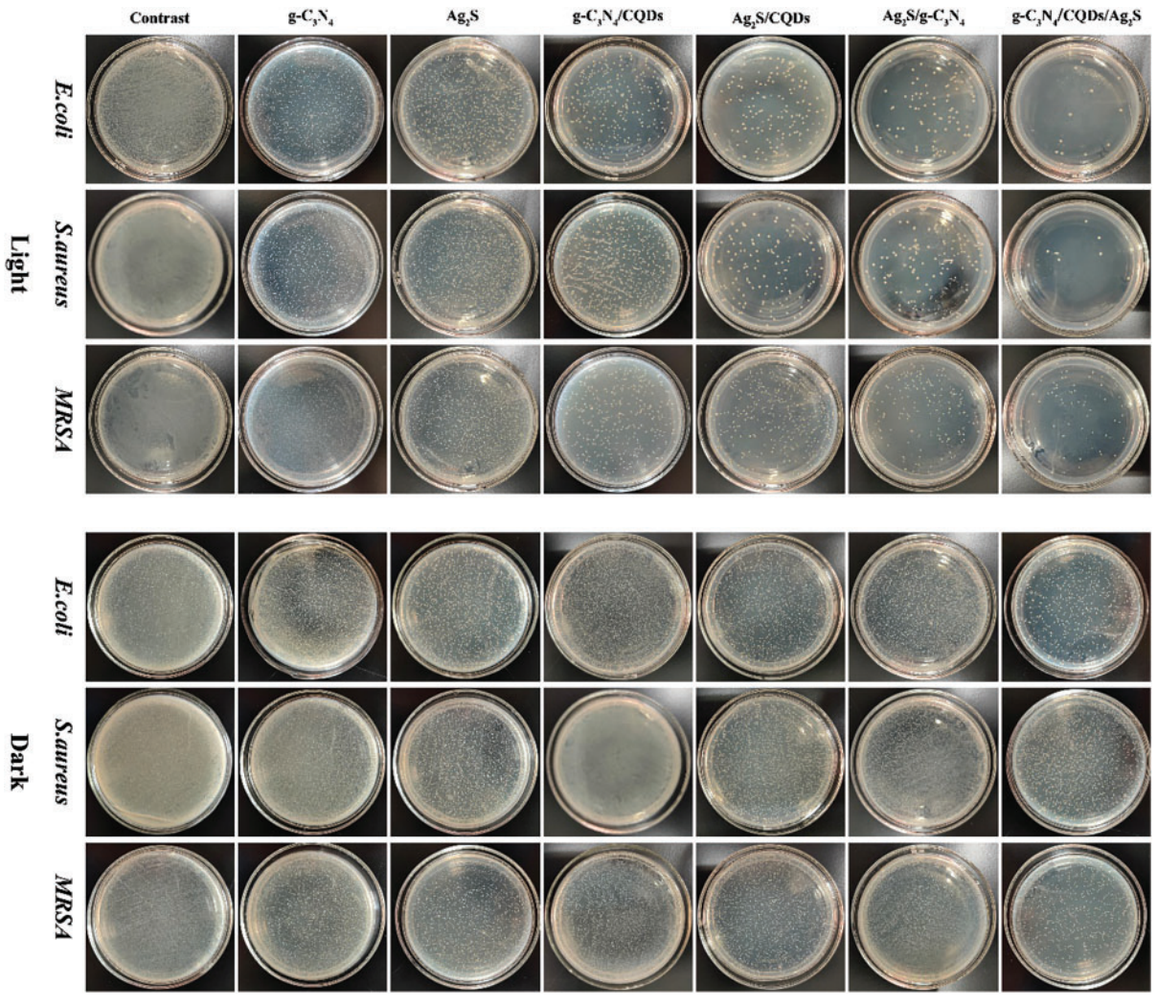

Fig. 8. *In vitro* antibacterial test of *E. coli*, *S. aureus* and MRSA under light or dark conditions.

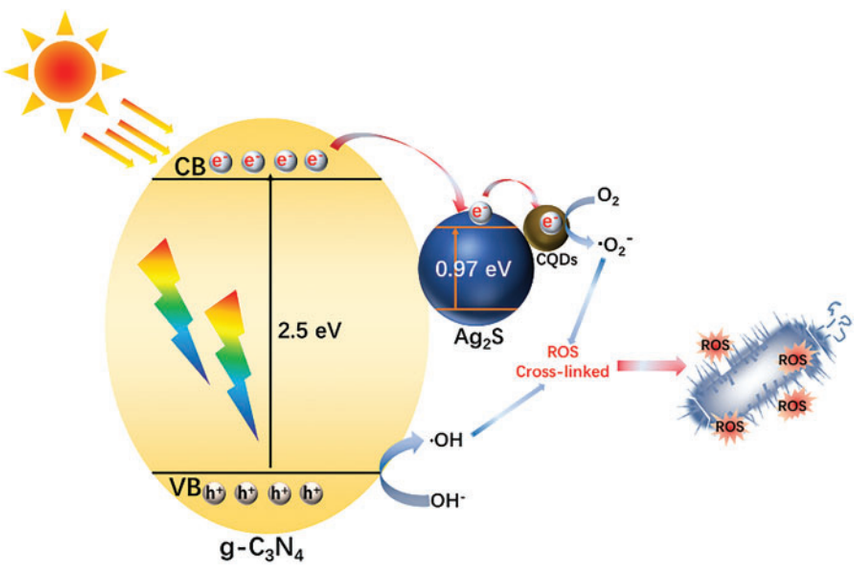

Fig. 9. Antibacterial mechanism of g-C_3N_4/CQDs/Ag_2S.

RESEARCH ARTICLE

shows for pure Ag_2S and g-C_3N_4, photo-generated electrons and holes are easy to recombine leading to a relatively low photocatalytic activity. In general, photocatalytic performance depends on two key characteristics, namely, the efficiency of utilizing the light, especially the visible light, and the population of photogenerated electrons and holes. Relatively long lived photoinduced charge carriers, such as holes may interact with the bacterial cell membrane based on their positive charge and further lead to the cell membrane rupture and death.[48] In other cases, photoinduced charge carriers react with water or dissolved oxygen to generate ROS to bring oxidizing stress to cell membrane, which either leads the rapture of cell membrane, or apply significant impact to the activities of various proteins that are of importance in the cell growth.[49,50] The present work greatly improves the photocatalytic activity of g-C_3N_4/CQDs/Ag_2S composite by elongating the lifetime of photoinduced electron–hole pairs through a heterostructure formed by the distribution of particles of CQDs Ag_2S on a flake-like surface of g-C_3N_4. These long lived photoinduced electron–hole pairs lead to significant production of ROS to fulfill the inhibition against bacterial growth.

4. CONCLUSION

We prepared g-C_3N_4 by simple heating treatment of melamine in air. The produced g-C_3N_4 was then compounded with Ag_2S and CQDs to develop g-C_3N_4/CQDs/Ag_2S composite material. A heterostructure established by loading Ag_2S and CQDs on the g-C_3N_4 significantly enhanced the light absorption efficiency and effectively prevented the recombination of the photoinduced electron–hole pairs. Therefore, the as prepared g-C_3N_4/CQDs/Ag_2S composite material exhibited an excellent antimicrobial effect against *Escherichia coli*, *Staphylococcus aureus* and methicillin-resistant *Staphylococcus aureus* after 4-hour light irradiation. Such antimicrobial effect was attributed to the photocatalytic activity of binding rate of the photo-generated electron holes of g-C_3N_4 is reduced, and the g-C_3N_4/CQDs/Ag_2S composite, a material that shows potential both in the development of antimicrobial agents and the materials with photocatalytic activities.

Ethical Compliance

Research experiments conducted in this article with animals or humans were approved by the Ethical Committee and responsible authorities of our research organization(s) following all guidelines, regulations, legal, and ethical standards as required for humans or animals.

Conflicts of Interest

The authors declare no conflicts of interest.

Acknowledgments: This work was supported by the National Nature Science Foundations of China (Grant Nos. 21867015, 22065021), the Key Research Program of Gansu Province (21YF5GA076), the Province Nature Science Foundations of Gansu (Grant Nos. 20JR5RA453, 21JR7RA213) and Hongliu Outstanding Youth Teacher Cultivate Project of Lanzhou University of Technology. HF thanks Nazarbayev University small grant 110119FD4542.

References and Notes

1. N. Kumar, A. Mittal, M. Yadav, et al., Photocatalytic TiO_2/CdS/ZnS nanocomposite induces bacillus subtilis cell death by disrupting its metabolism and membrane integrity. *Indian J. Microbiol.* 61, 487 **(2021)**.
2. S. V. Otari, S. K. S. Patel, V. C. Kalia, et al., Antimicrobial activity of biosynthesized silver nanoparticles decorated silica nanoparticles. *Indian J. Microbiol.* 59, 379 **(2019)**.
3. S. K. S. Patel, J. H. Kim, V. C. Kalia, et al., Antimicrobial activity of amino-derivatized cationic polysaccharides. *Indian J. Microbiol.* 59, 96 **(2019)**.
4. C. Mao, Y. Xiang, X. Liu, et al., Repeatable photodynamic therapy with triggered signaling pathways of fibroblast cell proliferation and differentiation to promote bacteria-accompanied wound healing. *ACS Nano* 12, 1747 **(2018)**.
5. F. Vatansever, W. C. De Melo, P. Avci, et al., Antimicrobial strategies centered around reactive oxygen species-bactericidal antibiotics, photodynamic therapy, and beyond. *FEMS Microbiol. Rev.* 37, 955 **(2013)**.
6. L. Carbone and P. D. Cozzoli, Colloidal heterostructured nanocrystals: Synthesis and growth mechanisms. *Nano Today* 5, 449 **(2010)**.
7. J. Tian, Y. Leng, Z. Zhao, et al., Carbon quantum dots/hydrogenated TiO_2 nanobelt heterostructures and their broad spectrum photocatalytic properties under UV, visible, and near-infrared irradiation. *Nano Energy* 11, 419 **(2015)**.
8. C. Hu, Y. Lan, J. Qu, et al., Ag/AgBr/TiO_2 visible light photocatalyst for destruction of azodyes and bacteria. *J. Phys. Chem. B* 110, 4066 **(2006)**.
9. L. Kőrösi, B. Bognár, M. Horváth, et al., Hydrothermal evolution of PF-Co-doped TiO_2 nanoparticles and their antibacterial activity against carbapenem-resistant klebsiella pneumoniae. *Appl. Catal. B* 231, 115 **(2018)**.
10. G. Xie, K. Zhang, B. Guo, et al., Graphene-based materials for hydrogen generation from light-driven water splitting. *Adv. Mater.* 25, 3820 **(2013)**.
11. O. K. Dalrymple, E. Stefanakos, M. A. Trotz, et al., A review of the mechanisms and modeling of photocatalytic disinfection. *Appl. Catal. B* 98, 27 **(2010)**.
12. C. Mutalik, D.-Y. Wang, D. I. Krisnawati, et al., Light-activated heterostructured nanomaterials for antibacterial applications. *Nanomaterials* 10, 643 **(2020)**.
13. S. Cao, J. Low, J. Yu, et al., Polymeric photocatalysts based on graphitic carbon nitride. *Adv. Mater.* 27, 2150 **(2015)**.
14. B. Song, Z. Zeng, G. Zeng, et al., Powerful combination of g-C_3N_4 and LDHs for enhanced photocatalytic performance: A review of strategy, synthesis, and applications. *Adv. Colloid Interfac.* 272, 101999 **(2019)**.
15. Y. Ni, R. Wang, W. Zhang, et al., Graphitic carbon nitride (g-C_3N_4)-based nanostructured materials for photodynamic inactivation: Synthesis, efficacy and mechanism. *Chem. Eng. J.* 404, 126528 **(2021)**.
16. S. Ma, S. Zhan, Y. Xia, et al., Enhanced photocatalytic bactericidal performance and mechanism with novel Ag/ZnO/g-C_3N_4 composite under visible light. *Catal. Today* 330, 179 **(2019)**.

RESEARCH ARTICLE

17. G. Mamba and A. Mishra, Graphitic carbon nitride (g-C_3N_4) nanocomposites: A new and exciting generation of visible light driven photocatalysts for environmental pollution remediation. *Appl. Catal. B* 198, 347 **(2016)**.

18. A. Sudhaik, P. Raizada, P. Shandilya, et al., Review on fabrication of graphitic carbon nitride based efficient nanocomposites for photodegradation of aqueous phase organic pollutants. *J. Ind. Eng. Chem.* 67, 28 **(2018)**.

19. J. Zhang, M. Zhang, R. Q. Sun, et al., A facile band alignment of polymeric carbon nitride semiconductors to construct isotype heterojunctions. *Angew. Chem. Int. Edit.* 51, 10145 **(2012)**.

20. W. S. Lee, Y. S. Park, and Y. K. Cho, Significantly enhanced antibacterial activity of TiO_2 nanofibers with hierarchical nanostructures and controlled crystallinity. *Analyst* 140, 616 **(2015)**.

21. V. Sivaranjani and P. Philominathan, Synthesize of titanium dioxide nanoparticles using moringa oleifera leaves and evaluation of wound healing activity. *Wound Medicine* 12, 1 **(2016)**.

22. K. Gupta, R. Singh, A. Pandey, et al., Photocatalytic antibacterial performance of TiO_2 and Ag-doped TiO_2 against *S. aureus*, *P. aeruginosa* and *E. coli*. *Beilstein J. Nanotech.* 4, 345 **(2013)**.

23. D. Wodka, E. Bielanska, R. P. Socha, et al., Photocatalytic activity of titanium dioxide modified by silver nanoparticles. *ACS Appl. Mater. Inter.* 2, 1945 **(2010)**.

24. P. Lu, X. Hu, Y. Li, et al., Novel $CaCO_3$/g-C_3N_4 composites with enhanced charge separation and photocatalytic activity. *J. Saudi Chem. Soc.* 23, 1109 **(2019)**.

25. P. Zeng, X. Ji, Z. Su, et al., WS2/gC_3N_4 composite as an efficient heterojunction photocatalyst for biocatalyzed artificial photosynthesis. *RSC Adv.* 8, 20557 **(2018)**.

26. L. A. L. Thi, M. M. Neto, T. P. Van, et al., In situ gC [sub. 3] N [sub. 4]@Zno nanocomposite: One-pot hydrothermal synthesis and photocatalytic performance under visible light irradiation. *Adv. Mater. Sci. Eng.* 2021 **(2021)**.

27. H. Lan, L. Li, X. An, et al., Microstructure of carbon nitride affecting synergetic photocatalytic activity: Hydrogen bonds vs. structural defects. *Appl. Catal. B* 204, 49 **(2017)**.

28. P. Murugesan, J. Moses, and C. Anandharamakrishnan, Photocatalytic disinfection efficiency of 2D structure graphitic carbon nitride-based nanocomposites: A review. *J. Mater. Sci.* 54, 12206 **(2019)**.

29. J. Chen, S. Shen, P. Guo, et al., In-situ reduction synthesis of nanosized Cu_2O particles modifying g-C_3N_4 for enhanced photocatalytic hydrogen production. *Appl. Catal. B* 152, 335 **(2014)**.

30. J. Zhang, F. Guo, and X. Wang, An optimized and general synthetic strategy for fabrication of polymeric carbon nitride nanoarchitectures. *Adv. Funct. Mater.* 23, 3008 **(2013)**.

31. J. Gao, C. Wu, D. Deng, et al., Direct synthesis of water-soluble aptamer-Ag_2S quantum dots at ambient temperature for specific imaging and photothermal therapy of cancer. *Adv. Healthc. Mater.* 5, 2437 **(2016)**.

32. X. Guo, W. Q. Ji, C. F. Wang, et al., Herbages-derived fluorescent carbon dots and CdTe/carbon ensembles for patterning. *J. Mater. Sci.* 51, 8108 **(2016)**.

33. S. Sharma, V. Dutta, P. Singh, et al., Carbon quantum dot supported semiconductor photocatalysts for efficient degradation of organic pollutants in water: A review. *J. Clean Prod.* 228, 755 **(2019)**.

34. K. Akbar, E. Moretti, and A. Vomiero, Carbon dots for photocatalytic degradation of aqueous pollutants: Recent advancements. *Adv. Opt. Mater.* 2100532 **(2021)**.

35. X. Gao, H. Li, X. Niu, et al., Carbon quantum dots modified Ag_2S/CS nanocomposite as effective antibacterial agents. *J. Inorg. Biochem.* 111456 **(2021)**.

36. H. Niu, W. Zhao, H. Lv, et al., Accurate design of hollow/tubular porous g-C_3N_4 from melamine-cyanuric acid supramolecular prepared with mechanochemical method. *Chem. Eng. J.* 411, 128400 **(2021)**.

37. K. Wang, Q. Ji, H. Li, et al., Synthesis and antibacterial activity of silver@carbon nanocomposites. *J. Inorg. Biochem.* 166, 64 **(2017)**.

38. W. Li, Q. Chen, and Q. Zhong, One-pot fabrication of mesoporous g-C_3N_4/NiS Co-catalyst counter electrodes for quantum-dot-sensitized solar cells. *J. Mater. Sci.* 55, 10712 **(2020)**.

39. Arne, Thomas, Anna, et al., Graphitic carbon nitride materials: Variation of structure and morphology and their use as metal-free catalysts. *J. Mater. Chem.* 18, 4893 **(2008)**.

40. Lei, Ge, Fan, et al., Synthesis and efficient visible light photocatalytic hydrogen evolution of polymeric g-C_3N_4 coupled with CdS quantum dots. *J. Phys. Chem. C* 116, 13708 **(2012)**.

41. Y. Sun, R. Li, R. Xu, et al., Chemically converted graphene as substrate for immobilizing and enhancing the activity of a polymeric catalyst. *Chem. Commun.* 46, 4740 **(2010)**.

42. Y. S. Xu and W. D. Zhang, Ag/AgBr-grafted graphite-like carbon nitride with enhanced plasmonic photocatalytic activity under visible light. *Chemcatchem* 5, 2540 **(2013)**.

43. Z. Liu, Z. Mo, X. Niu, et al., Highly sensitive fluorescence sensor for mercury (II) based on boron-and nitrogen-co-doped graphene quantum dots. *J. Colloid Interf. Sci.* 566, 357 **(2020)**.

44. C. Wang, H. Shi, M. Yang, et al., Biocompatible sulfur nitrogen Co-doped carbon quantum dots for highly sensitive and selective detection of dopamine. *Colloid Surface B* 205, 111874 **(2021)**.

45. V. Colvin, A. Goldstein, and A. Alivisatos, Semiconductor nanocrystals covalently bound to metal surfaces with self-assembled monolayers. *J. Am. Chem. Soc.* 114, 5221 **(1992)**.

46. H. Yu, W. Liu, X. Wang, et al., Promoting the interfacial H_2-evolution reaction of metallic Ag by Ag_2S cocatalyst: A case study of TiO_2/Ag–Ag_2S photocatalyst. *Appl. Catal. B* 225, 415 **(2018)**.

47. D. Jiang, L. Chen, J. Zhu, et al., Novel p–n heterojunction photocatalyst constructed by porous graphite-like C_3N_4 and nanostructured BiOI: Facile synthesis and enhanced photocatalytic activity. *Dalton T.* 42, 15726 **(2013)**.

48. W. Naim, O. R. Schade, E. Saraci, et al., Toward an intensified process of biomass-derived monomers: The influence of 5-(hydroxymethyl) furfural byproducts on the gold-catalyzed synthesis of 2,5-furandicarboxylic acid. *ACS Sustain. Chem. Eng.* 8, 11512 **(2020)**.

49. C. Regmi, B. Joshi, S. K. Ray, et al., Understanding mechanism of photocatalytic microbial decontamination of environmental wastewater. *Front. Chem.* 6, 33 **(2018)**.

50. H. Park, E. T. Bentria, S. Rtimi, et al., Accelerating the design of photocatalytic surfaces for antimicrobial application: Machine learning based on a sparse dataset. *Catalysts* 11, 1001 **(2021)**.

Received: 22 January 2022. Accepted: 5 March 2022.

RESEARCH ARTICLE